Audio Engineering Society

Convention Paper 9679

Presented at the 141st Convention
2016 September 29 – October 2, Los Angeles, CA, USA

Physically Derived Synthesis Model of an Aeolian Tone

Rod Selfridge[1], Joshua D Reiss[1], Eldad J Avital[2], and Xiaolong Tang[2]

[1]*Centre for Digital Music, School of EECS, Queen Mary University of London, E1 4NS, U.K*
[2]*Centre for Simulation and Applied Mechanics, School of EMS, Queen Mary University of London, E1 4NS, U.K*

Correspondence should be addressed to Rod Selfridge (r.selfridge@qmul.ac.uk)

ABSTRACT

An Aeolian tone is the whistle-like sound that is generated when air moves past a cylinder or similar object; it is one of the primary aeroacoustic sound sources. A synthesis model of an Aeolian tone has been developed based on empirical formula derived from fundamental fluid dynamics equations. It avoids time consuming computations and allows real-time operation and interaction. Evaluation of the synthesis model shows frequencies produced are close to those measured in a wind tunnel or simulated through traditional offline computations.

Nomenclature

c = speed of sound (ms^{-1})

d = diameter (m)

f = frequency (Hz)

u = air flow speed (ms^{-1})

R_e = Reynolds number (dimensionless)

S_t = Strouhal number (dimensionless)

r = distance between listener and sound source (m)

θ° = elevation angle between listener and sound source

φ° = azimuth angle between listener and sound source

ρ_{air} = mass density of air (kgm^{-3})

μ_{air} = dynamic viscosity of air ($Pa\,s$)

M = Mach number (dimensionless)

l = correlation length of cylinder (diameters)

b = length of cylinder (m)

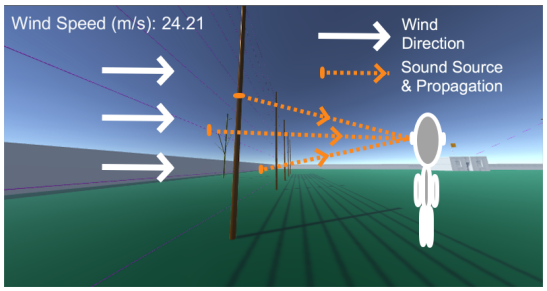

Fig. 1: Winds blowing though a fence can produce an Aeolian tone.

1 Introduction

Aeroacoustic sounds are the class of sounds that are generated by the movement of air passed objects or edges. Alternatively, the sounds can also be generated by objects moving through the air. Examples of aeroacoustic sounds are those created when a sword swings through the air, wind passes a doorway or a spinning propellor. A visual representation of an Aeolian tone from wind passing a wire fence is given in Fig. 1.

Research is undertaken to accurately determine the frequencies, gain, propagation patterns required to replicate the Aeolian tone. Key empirical formula are found within in the aeroacoustic research field, allowing us to identify key relationships and parameters. A major advantage of a physical model is that users can change parameters and be confident that the underlying laws and principles are consistently obeyed, giving sounds produced an inherent authenticity.

Our model has applications within video games, films or television post production. The model is classified within *Procedural Audio*; each sound produced is unique, based on the current situation, i.e. speed of air/object motion, observer or camera position, etc. Parameters can be manipulated by a user, producing instant changes in real-time or full automated by a game engine.

The goal is to create a model of what is known in the aeroacoustics field as a compact sound source. Physics will be at the core of the synthesis process and operation to be in real-time. For a given cylinder it would be possible to predict the sound generated. Models to generate the physical characteristics of the wind, including fluctuations or replicate the swing of a sword are not within the scope of this paper.

2 State of the Art

Physical models are one of a number of synthesis techniques that can be used to generate sound effects. Others include additive, granular, subtractive and modal. A comprehensive review of synthesis techniques is given in [1]. When generating a physical model it is common to discretise the materials in question; finite element techniques for solids and finite volume techniques for fluids, techniques requiring offline computations. Finite element techniques are used in [2], [3] and [4] to solve the linear elastodynamic equation giving the natural frequency of nodes within the structure.

A comparison of wind and sword sounds based on the Aeolian tone is presented in Table 1. The table specifies different synthesis techniques, including ones that use offline finite volume techniques.

Noise shaping was used in [5] and [6] to generate whistling wind sounds, varying the centre frequency of a bandpass filter proportional to the wind speed. Both synthesis models operate in real-time and replicate some of the underlying physics; they do not calculate the exact frequency nor take into account factors such as the diameter of the interacting object or the relationship between listener and source.

In [7] a Computational Fluid Dynamics (CFD) approach was taken to calculate the Aeolian tones. A finite volume computational method was applied to solve the fundamental fluid motion equations, (Euler equations), for air passing a cylinder; cylinder diameter and incoming flow speed controlled by the user. The results have a far greater accuracy than [5] and [6] but sounds require offline processing to realise and the model can not react to changing conditions. A full simulation is required for each specific parameter change.

The sound of a sword swinging through the air is synthesised in [8] using CFD techniques. Here the Aeolian tones are generated by solving the Navier Stokes equations. Using *Lighthill's acoustic analogy*, [9], extended by *Curle's Method*, [10], the sounds are predicted. The sword is discretised into a number of *compact sources* dependent on the shape and size of the sword.

Four different synthesis techniques for generating the swoosh sound of a sword were evaluated in [11] for perception and preference. Models included a band filtered noise signal with the centre frequency proportional to the acceleration of the controller, similar to the noise shaped wind models above. A physically inspired model reproduced the dominant frequency modes recorded from a bamboo stick swung through the air; acceleration mapped to mode amplitude in real-time. The other synthesis methods both mapped acceleration to different parameters; one threshold between two audio samples, the other is a granular synthesis method mapping acceleration to playback speed thought the grains. Tests revealed the granular synthesis was preferred.

3 Background Theory of Aeolian Tone

A diagram indicating the coordinates and parameters used throughout is shown in Fig. 2.

3.1 Tone Frequency

Strouhal, (1878), defined a useful relationship between the tone frequency, air speed and cylinder diameter:

Table 1: Comparison of different Aeolian tone (or similar) synthesis

Effect	Control	Method	Computation	Physics Used	Assumptions	Reference
Wind	d, r, θ, φ , u, b	Physical model	Real-time	Empirical equations (see text)	See Section 4	Proposed method
	Proof of concept	Noise shaping		Filter centre frequency & gain $\propto u$.	Parameter ratios, uniform radiation & single tone	[5]
	u			Filter centre frequency $\propto u$	Preset values for wind type	[6]
	u, d, & boundary conditions	CFD	Offline	Euler equations	None	[7]
Sword	Speed of motion		Offline / Real-time	Navier Stokes equations and Curle's method	None	[8]
		Modal Synthesis	Offline / Real-time	Mode amplitude $\propto$ acceleration	Frequency modes fixed	[11]

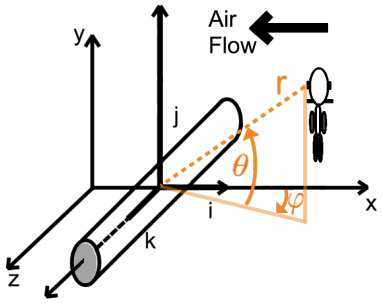

Fig. 2: Coordinate system used for sound emission from a cylinder.

$$S_t = \frac{f\,u}{d} \tag{1}$$

As air passes the cylinder vortices are shed from opposite sides at the given fundamental frequency. This causes a fluctuating lift force dominated by the fundamental frequency of $S_t \simeq 0.2$, f_l. Simultaneously a side axial drag force is present as air flows round the cylinder and its fluctuations are dominated by $S_t \simeq 0.4$, f_d. In [12] it is noted that the amplitude of this drag force is approximately one tenth the amplitude of the lift force.

It was shown in [10] and confirmed in [13] that aeroacoustic sounds, in low flow speed situations, could be modelled by the summation of compact sources, namely monopoles, dipoles and quadrupoles. Aeolian tones can be represented by dipole sources for the lift fundamental frequency, drag fundamental frequency as well as a number of harmonics. The acoustic output for ideal lift and drag dipole sources is illustrated in Fig. 3. As depicted, it can be seen that the major sound source is the lift dipole which is perpendicular to the flow direction. The drag dipole is parallel to the flow direction and has a much smaller influence on the final sound.

The sound generated is strongly influenced by the turbulence generated as air flows past the cylinder; the more turbulent the flow the more diffused the vortices will be. Turbulence is indicated by the Reynolds number which is given in Eq. (2):

$$R_e = \frac{\rho_{air}\,d\,u}{\mu_{air}} \tag{2}$$

An experimental study of the relationship between fundamental Strouhal number, (associated with the lift force), and Reynolds number was performed in [14], giving the following relationship:

$$S_t = \lambda + \frac{\tau}{\sqrt{R_e}} \tag{3}$$

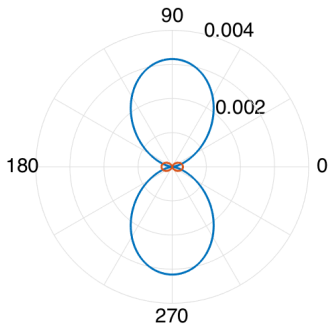

Fig. 3: Ideal radiation patterns for perpendicular dipole sources - lift (blue) and drag (red). u = 69m/s, d = 0.019m, r = 12m, Units for $I = W/m^2$. (The flow direction is from 0° to 180°)

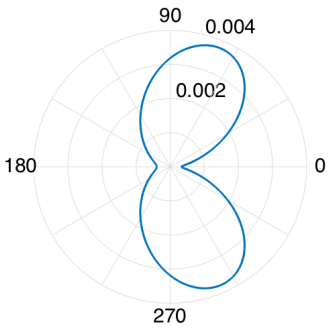

Fig. 4: Composite of lift, drag and turbulence sound sources with M = 0.2. u = 69m/s, d = 0.019m, r = 12m, Units for $I = W/m^2$. (The flow direction is from 0 ° to 180 °)

Table 2: Values for constants in Eq.(3), reproduced from [14]. † Linear interpolation between published values. ‡ interpolated from [17].

R_e **range**	λ	τ
[47,180)	0.2684	-1.0356
[180, 230)	0.2437	-0.8607
[230, 240)	0.4291	-3.6735
[240, 360)	0.2492†	-0.8861†
[360, 1300)	0.2257	-0.4402
[1300, 5000)	0.2040	+0.3364
[5000, 2x10^5)	0.1776	+2.2023
[2x10^5, 1x10^6)	0.5760‡	-175.956‡

where λ and τ are constants and given in Table 2. The different values represents the transition regions of the flow, starting at laminar up to sub-critical turbulence. When the Reynolds number lies between $2*10^5$ and $1.0*10^6$ it enters its *Critical* region. Here the Strouhal number jumps to values of approximately 0.45, [15], [16] and [17]. Above this region it returns to values similar to the subcritical region, ~ 0.2. No values were published for this region in [14].

Using Eq. (2) to calculate R_e we can use Eq. (3) to obtain S_t. All parameters are then available to calculate the fundamental frequency of the aeolian tone, Eq. (1).

3.2 Source Gain

The time-averaged Acoustic Intensity $\overline{I_l(t)}$ (W/m^2), of an Aeolian tone lift dipole source is given in [18] as:

$$\overline{I_l(t)} \sim \frac{\sqrt{2\pi}\kappa^2 S_t^2 l\ b\ \rho\ u^6 sin^2\theta cos^2\varphi}{32c^3 r^2 (1-Mcos\theta)^4} \left\{ exp\left[-\frac{1}{2}\left(\frac{2\pi M S_t l}{d}\right)^2 sin^2\theta sin^2\varphi \right] \right\} \quad (4)$$

where κ is a constant between 0.5 and 2. The correlation length, l, given in diameters, indicates the length that the vortex shedding is in phase. The averaging time period T_p is given as:

$$T_p = \frac{2\pi}{f_l}(1-Mcos\theta) \quad (5)$$

The Mach number has a large effect on the peak propagation angle of the lift dipole; the higher the Mach number the more upstream the peak propagation angle. When the Mach number is low, $M << 1$, the Doppler factor within Eq. (4), $\{exp[....]\}$, can be neglected. Fig. 4 shows the resultant propagation pattern from combining the fundamental sources.

3.3 Harmonic Content

A number of publications, including [13] and [17], indicate that harmonics of the fundamental frequency are present in the Aeolian tone. Normalised gains for the harmonics are given in [19]. The amplitude of the fundamental frequency and harmonics are related to the *turbulence intensity* of the incoming free stream of air but the difference appears minimal given plots presented in [20].

3.4 Tone Bandwidth

The bandwidth around the fundamental frequency is effected by the Reynolds number, [21]. Data published is for the range of Reynolds numbers from 0 to 237,000 and for turbulence intensity for 0.1% and 1.4%. The range of $\Delta f/f$ is approximately 0% to 10%.

3.5 Wake Noise

The Aeolian tone is virtually a single sine wave at low Reynolds numbers. When the Reynolds number increases, the vortices produce diffuses rapidly and the individual vortices merge into a turbulent wake. The wake produces wide band noise modelled by lateral quadrupole sources whose intensity varies with the power of 8, [22].

It is also noted in [22] was that there is very little noise content below the lift dipole fundamental frequency. Further, it was shown in [23] that the roll off of the amplitude of the turbulent noise, above the fundamental frequency is $\frac{1}{f^2}$.

The sound generated by turbulence is examined in [18]. Here it states radiated sound pattern is greatly influenced by a Doppler factor of $(1-Mcos\theta)^{-5}$. The wake noise intensity, $\overline{I_w(t)}$, has been approximated by the authors to capture this relationship as shown in Eq. 6[1]:

$$\overline{I_w(t)} \sim \frac{\sqrt{2\pi}\kappa^2 S_t^2 l\ b\rho\ u^8}{16\pi^2 c^5 (1-Mcos(180-\theta))^5 r^2} \qquad (6)$$

4 Implementation

Our model was realised in Pure Data an open source real-time graphical data flow programming language.

4.1 Fundamental Frequency Calculation

A uniform sampling of the continuous air flow speed, u is used to obtain the Reynolds number $R_e[n]$, at sample n. The relationship in Eq. (3) and data from Table 2 produces a discrete Strouhal number, $S_t[n]$. For a given diameter, d, a discrete time implementation of Eq.(1 enables us to obtain a value for the lift dipole fundamental frequency, $f_l[n]$. The frequency values for the drag dipole and harmonics are then calculated as indicated in Table 3.

As stated in section 3.4, there is a bandwidth around the fundamental frequency and this is related to the Reynolds number and the free stream turbulence. Data available in [21] was limited to turbulence intensity of 0.1% and 1.4% as well as Reynolds numbers under 237,000. Due to the lack of data the dependancy on turbulence intensity was not implemented. The relationship between the bandwidth and Reynolds number from 0 to 193,260 was found to be linear. This relationship was interpolated from the data as:

$$\frac{\Delta f}{f_l}(\%) = 4.624 * 10^{-5} R_e + 0.9797 \qquad (7)$$

After a Reynolds number of 193,260 a quadratic formula found to fit the bandwidth data. This is shown in Eq. (8):

$$\frac{\Delta f}{f_l}(\%) = 1.27 * 10^{-10} R_e^2 - 8.552 * 10^{-5} R_e + 16.5 \qquad (8)$$

The Q value of a filter is given as $f_l/\Delta f$, the reciprocal of the percentage value obtained by a discrete implementation of equations 7 and 8, (divided by 100 and inverted). To generate the correct sound a band-pass filter with varying centre frequency matching the fundamental lift frequency and Q value calculated in real-time, proportional to $R_e[n]$. This is duplicated to generate sound for the drag fundamental frequency as well as the harmonics.

4.2 Gain Calculations

The dipole source of Eq. (4) pertains to the lift force and is implemented to give a discrete time-averaged intensity value $\overline{I_l[n]}$, taking $\kappa = 1$. A graph published in [24] shows the ratio of correlation length to diameter, l/d, as a function of the Reynolds number. An equation replicating this relationship has been derived, Eq. (9):

$$l = 10^{1.536}.\ R_e[n]^{-0.245}.\ d \qquad (9)$$

The discrete intensity value pertaining to the drag force is calculated in Eq. (10):

[1] $180-\theta$ is employed due to difference in flow direction used in [18].

Harmonic	f_i	$\overline{I_i(t)}$
Drag dipole fundamental (f_d)	$2f_l(t)$	$0.1\overline{I_l(t)}$
Lift dipole 1st harmonic	$3f_l(t)$	$0.6\overline{I_l(t)}$
Drag dipole 1st harmonic	$4f_l(t)$	$0.0125\overline{I_l(t)}$
Lift dipole 2nd harmonic	$5f_l(t)$	$0.1\overline{I_l(t)}$

Table 3: Additional frequencies and gains as a function of the lift dipole fundamental frequency $f_l(t)$.

$$\overline{I_d[n]} \sim 0.1 \frac{\sqrt{2\pi}S_t[n]^2 lb\rho u[n]^6 (sin(\theta+\frac{\pi}{2}))^2 (cos\varphi)^2}{32c^3 r[n]^2} \tag{10}$$

A constant $\frac{\pi}{2}$ is added to the value of $\theta[n]$ due to the 90° phase difference between the lift and drag forces. Compared with Eq. (4), there is no perpendicular flow therefore M was set to 0. The time averaging period was implemented with a discrete form of Eq. (5).

4.3 Harmonic Content Calculations

Subsection 3.3 states there are a number of harmonics present in the tone. We can calculate the drag dipole frequency and harmonics as shown in Table 3. The gain for the drag dipole is obtained from [12] and the lift dipole harmonics values from [19]. The drag dipole 1st harmonic was witnessed from computational simulations and added at the appropriate value.

4.4 Wake Calculations

A noise profile of $\frac{1}{f^2}$ is known as *Brown Noise*. This can be approximated using white noise and the transfer function shown in Eq. (11), [25]:

$$H_{brown}(z) = \frac{1}{1-\alpha z^{-1}} \tag{11}$$

The required noise profile is generated using the transfer function given in Eq. (13):

$$B[z] = H_{brown}[z]W[z] \tag{12}$$

where W[z] is a white noise source and the output $B[z]$ is a brown noise source.

In [25] α has a value of 1 but this proved unstable in our implementation and a value of 0.99, producing virtually identical output, was chosen. As found in [22] there is little wake contribution below the fundamental frequency therefore a high pass filter is applied to $B[z]$ with the filter cut off set at the lift dipole fundamental frequency, $f_l[n]$. This gives the turbulent noise profile required, $G[z]$:

$$G[z] = H_{hp}[z]B[z] \tag{13}$$

where $H_{hp}[z]$ is the high pass filter transfer function. The inverse Z-transform of $G[z]$ gives the wake output signal, $g[n]$. A discrete implementation of the wake noise intensity given in Eq. (6) gives $\overline{I_w[n]}$.

4.5 Final Output

Combining the outputs from the harmonics and wake sources it is possible to derive a final output. For the lift dipole we have the outputs of the bandpass filters, $b_{l1}[n]$, $b_{l3}[n]$, $b_{l5}[n]$, centred at f_l, $3f_l$ and $5f_l$, gains set at $\overline{I_l[n]}$, $0.6\overline{I_l[n]}$ and $0.1\overline{I_l[n]}$ respectively.

Similarly the drag dipole has output from bandpass filters $b_{d1}[n]$, $b_{d2}[n]$, centred at f_d and $2f_d$ with gains of $\overline{I_d[n]}$, $0.125\overline{I_d[n]}$ respectively.

Finally there is the wake output $g[n]$ with gain $\overline{I_w[n]}$ giving the final output, Eq. (14):

$$\begin{aligned} y_{output}[n] &= \overline{I_l[n]}\Big[b_{l1}[n] + 0.6b_{l3}[n] + 0.1b_{l5}[n]\Big] \\ &+ \overline{I_d[n]}\Big[b_{d1}[n] + 0.125b_{d2}[n]\Big] + \overline{I_w[n]}g[n] \end{aligned} \tag{14}$$

4.6 Limitations

In our model we have derived the equation for the intensity of the wake, Eq. (6) from principals described in [18]. This and Eq. (4) both state the intensity is similar to ($\sim$) the given equation. Their relationship to each other is unknown but the wake noise is considerably lower than the dipole sounds, especially at low flow speeds.

In [21] the relationship between bandwidth and frequency is only published for the fundamental lift frequency. It is possible that the harmonics have a different relationship which is not captured by our model.

Bandwidth data is only published up to a Reynolds number of 237,000. Our model is able to operate above this and the relationship given by the best fit quadratic may not be accurate after this value.

5 Results and Discussion

A number of previous studies have published Aeolian tone frequency values at different air flow speeds and cylinder diameters. The conditions specified in these publications have been replicated in our model and the results noted in Table 4.

There are a number of discrepancies between the published values and values simulated by our model. Some general explanations go some way to explain these. Firstly, the wind tunnel experiments may be susceptible to noise from the measurement instruments themselves, calibration of instrumentation or even human errors. Some of the historical measurements date back to the 1950s and 1960s and measurement equipment will have improved greatly from this time.

In relation to our model, the fundamental frequency from the lift dipole relies on the relationship between the Reynolds number and Strouhal number taken from [14], which is a piecewise linear approximation. The published error is up to +/- 0.003 in the Strouhal number which related to approximately +/- 1.5% in frequency value. The free stream turbulence intensity is captured in the wind tunnel but not in our model. The roughness of the cylinder as well as mechanical vibrations are not considered by our model but are known to have influence over the wind tunnel results. Overall the differences between tone frequencies produced by our model and the published values are minor, the worst case being one of the historical papers.

To further verify our model conditions were replicated using the CFD software, Fluent. This would allow us to note similarities and differences with a commercial package operating offline. In these simulations we used the Unsteady Reynolds Averaged Navier Stokes (URANS), equations operating in 2 dimensions. The SST k-ω model was used on a mesh with 73728 elements, shown in Fig. 5. The numerical scheme was 2nd order upwind. The velocity vectors for a typical simulation is shown in Fig. 6. The vortex shedding can clearly be seen emerging from the rear of the cylinder.

Acoustic analysis was carried out using the built-in Ffowcs-Williams and Hawkings acoustical analysis

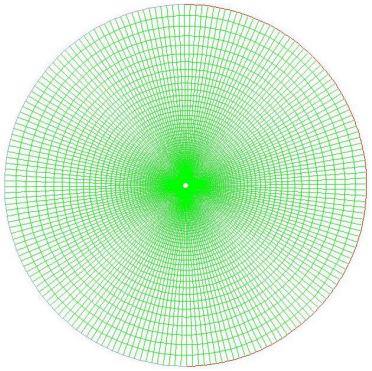

Fig. 5: Mesh used to solve the CFD problem in Fluent.

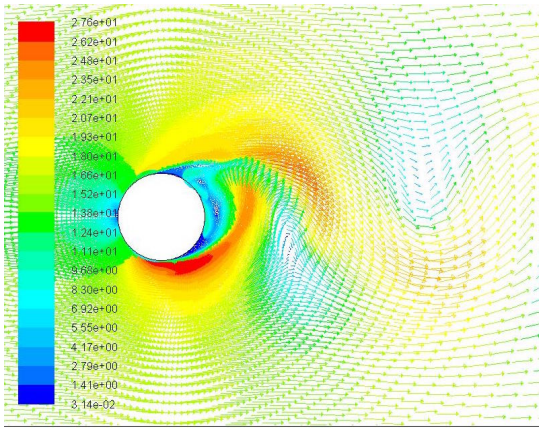

Fig. 6: Velocity vectors showing vortices being shed behind a cylinder.

method [30]. The acoustic receiver was positioned at a distance, $r = 12m$ and an elevation angle, $\varphi = 90°$. The differences between published results and those obtained from the CFD software are far greater than those obtained from our model. There are a number of reasons for these differences, including how the CFD software computes the interaction at the boundary of the cylinder and the main flow domain. Simulating the tones in 2 dimensions means we cannot fully simulate the turbulence which is a 3D phenomenon.

A closer examination of the output from our model and that of the CFD simulation can be seen in Fig. 7, replicating conditions from [27]. An obvious difference in the spectrum produced by the CFD software is it is virtually a pure tone, along with harmonics. There are no bandwidths as highlighted in [21], because Fluent simulations in 2D are not able to simulate the turbulent

Table 4: Comparison of known measured results, ones we have simulated using Fluent CFD and our synthesis model - (* read from a graph, ** computed answer); (a) [26], (b) [27], (c)[7], (d) [28] (e) [22], (f) [29]. (Frequencies are in Hz)

	(a)		(b)	(c)	(d)	(e)		(f)		
Air speed (m/s)	20	40	15	69	69	68.58	42.67	16.6	26.7	32.3
Diameter (m)	0.004	0.004	0.006	0.019	0.019	0.0127	0.0127	0.0254	0.0254	0.0254
Published Frequency	1000	2000*	508	617**	643	1000*	650*	150*	210*	240*
Real-Time Model Frequency	1038	1988	515	674	674	1008	635	125	197	238
Fluent CFD Frequency	1113	1635	590	837	837	1148	703	145	245	304

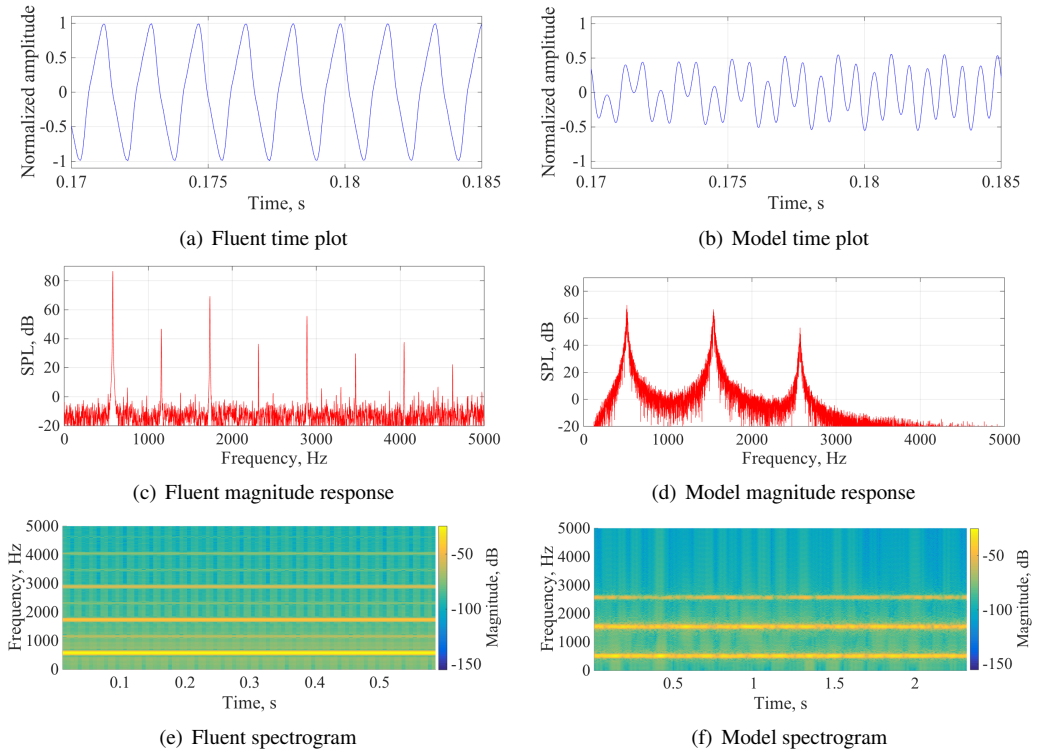

(a) Fluent time plot (b) Model time plot

(c) Fluent magnitude response (d) Model magnitude response

(e) Fluent spectrogram (f) Model spectrogram

Fig. 7: Fluent CFD and our model simulations, $u = 15$ m/s, $d = 0.006$ m.

structure cascade, but just capture the tones. The $\frac{1}{f^2}$ roll off will also not be visible. The lack of turbulence explains why the time plot in Fig. 7(a) is a sine wave. The time plot from out model, Fig. 7(b), has more variation, capturing the turbulence. This may well be a more accurate representation of the acoustic output than the 2D computation.

The magnitude spectrum of the Fluent simulation given in Fig. 7(c) clearly shows the fundamental, 3rd, 5th and 7th harmonics, associated with the oscillating lift force. Peaks can be seen in our model only at the fundamental, 3rd and 5th harmonics, Fig. 7(d). In Fig. 7(c) there are also peaks at the 2nd, 4th and 6th harmonics. These are associated with the drag force which have little amplitude at an elevation of 90°. These peaks are not visible in our model.

The spectrograms of Fig. 7(e) and 7(f) show clearly the difference in frequency values, most obvious for the 3rd and 5th harmonies. The 2nd, 4th, 6th, and 7th harmonies can also be seen in Fig. 7(e) but the magnitudes are low. The 2nd and 4th partials are included in our model but prevalent at an elevation of 0°. The inclusion of the 6th and 7th partials will increase the accuraty of our model but computationally expensive for virtually inaudible harmonics. In Fig. 7(f) there is a lot more noise content relating to the turbulence present in our synthesis model.

The accounting of turbulent structures by our model gives a more accurate representation of the fluid dynamics missing from 2D CFD simulations. Turbulence is missing in the sword model of [8] although they state this is perceived as unfavourable noise in the sound effect. A sword sound effect made with our model will include turbulence proportional to the Reynolds number and hence possibly create a more authentic sound effect.

6 Conclusions

We have developed a compact sound source representing the Aeolian tone based on empirical formulas from fundamental fluid dynamics equations. This has produced a sound synthesis model which closely represents what would be generated in nature. The model operates in real time and unlike other models, our approach accounts for the angle and distance between source and receiver.

An Aeolian tone compact source model can be used as a integral component of future aeroacoustic sound effects. This can include sounds generated by wind, Aeolian harps, swords swooshing through the air, axes and clubs being swung. It would also be possible to develop fan, propellor and turbine sound effects with the Aeolian tone a central component. This model has a validity when generating sounds for subsonic air speeds, $< 343\ m/s$. This makes it possible to model wind speeds that cannot be safely recorded or even wind speeds above those that occur naturally.

Discrepancies between our model and previously published results have been shown. The real-time synthesis model performs well at predicting the fundamental frequency of the previously published tones. Some turbulence effects are captured by our model missing the from 2D CFD simulation. Further developments for our model would be to the ability to adapt to different shapes and add in natural string harmonics to increase the accuracy and scope of objects that can be modelled.

References

[1] Schwarz, D., "State of the art in sound texture synthesis," in *Proc. Digital Audio Effects (DAFx)*, pp. 221–231, 2011.

[2] Zheng, C. and James, D. L., "Rigid-body fracture sound with precomputed soundbanks," in *ACM Transactions on Graphics (TOG)*, volume 29, p. 69, ACM, 2010.

[3] Zheng, C. and James, D. L., "Toward high-quality modal contact sound," *ACM Transactions on Graphics (TOG)*, 30(4), p. 38, 2011.

[4] Langlois, T. R., An, S. S., Jin, K. K., and James, D. L., "Eigenmode Compression for Modal Sound Models," *ACM Transactions on Graphics (TOG)*, 33(4), p. 40, 2014.

[5] Farnell, A., *Designing sound*, Mit Press Cambridge, 2010.

[6] Verron, C. and Drettakis, G., "Procedural audio modeling for particle-based environmental effects," in *Audio Engineering Society Convention 133*, 2012.

[7] Loh, C. Y. and Jorgenson, P. C., "Computation of tone noises generated in viscous flows," in *Proceedings of the 4th CAA Workshop on Benchmark Problems, NASA/CP-2004-212954*, volume 213, 2004.

[8] Dobashi, Y., Yamamoto, T., and Nishita, T., "Real-time rendering of aerodynamic sound using sound textures based on computational fluid dynamics," in *ACM Transactions on Graphics (TOG)*, volume 22, pp. 732–740, ACM, 2003.

[9] Lighthill, M. J., "On sound generated aerodynamically. I. General theory," *Proceedings of the Royal Society of London. Series A. Mathematical and Physical Sciences*, 211(1107), pp. 564–587, 1952.

[10] Curle, N., "The influence of solid boundaries upon aerodynamic sound," in *Proceedings of the Royal Society of London A: Mathematical, Physical and Engineering Sciences*, volume 231, pp. 505–514, 1955.

[11] Böttcher, N. and Serafin, S., "Design and evaluation of physically inspired models of sound effects in computer games," in *Audio Engineering Society Conference: 35th International Conference: Audio for Games*, 2009.

[12] Cheong, C., Joseph, P., Park, Y., and Lee, S., "Computation of aeolian tone from a circular cylinder using source models," *Applied Acoustics*, 69(2), pp. 110–126, 2008.

[13] Gerrard, J., "Measurements of the sound from circular cylinders in an air stream," *Proceedings of the Physical Society. Section B*, 68(7), p. 453, 1955.

[14] Fey, U., König, M., and Eckelmann, H., "A new Strouhal-Reynolds-number relationship for the circular cylinder in the range 47 105," *Physics of Fluids*, 10, pp. 1547–1549, 1998.

[15] Roshko, A., "Experiments on the flow past a circular cylinder at very high Reynolds number," *Journal of Fluid Mechanics*, 10(03), pp. 345–356, 1961.

[16] Lienhard, J. H., *Synopsis of lift, drag, and vortex frequency data for rigid circular cylinders*, Technical Extension Service, Washington State University, 1966.

[17] Fujita, H., "The characteristics of the Aeolian tone radiated from two-dimensional cylinders," *Fluid dynamics research*, 42(1), p. 015002, 2010.

[18] Goldstein, M. E., "Aeroacoustics," *New York, McGraw-Hill International Book Co., 1976. 305 p.*, 1, 1976.

[19] Hardin, J. C. and Lamkin, S. L., "Aeroacoustic Computation of Cylinder Wake Flow." *AIAA journal*, 22(1), pp. 51–57, 1984.

[20] Norberg, C., "Interaction between freestream turbulence and vortex shedding for a single tube in cross-flow," *Journal of wind engineering and industrial aerodynamics*, 23, pp. 501–514, 1986.

[21] Norberg, C., "Effects of Reynolds number and a low-intensity freestream turbulence on the flow around a circular cylinder," *Chalmers University, Goteborg, Sweden, Technological Publications*, 87(2), 1987.

[22] Etkin, B., Korbacher, G., and Keefe, R., "Acoustic radiation from a stationary cylinder in a fluid stream (Aeolian tones)," *The Journal of the Acoustical Society of America*, 29(1), pp. 30–36, 1957.

[23] Powell, A., "Similarity and turbulent jet noise," *The Journal of the Acoustical Society of America*, 31(6), pp. 812–813, 1959.

[24] Norberg, C., "Flow around a circular cylinder: aspects of fluctuating lift," *Journal of Fluids and Structures*, 15(3), pp. 459–469, 2001.

[25] Kasdin, N. J., "Discrete simulation of colored noise and stochastic processes and 1/f α power law noise generation," *Proceedings of the IEEE*, 83(5), pp. 802–827, 1995.

[26] Bazhenova, L. and Semenov, A., "Nature of the source of vortex sound flowing around a cylindrical profile," *Acoustical Physics*, 60(6), pp. 678–686, 2014.

[27] Uda, T., Nishikawa, A., Someya, S., and Iida, A., "Cross-correlation analysis of aeroacoustic sound and flow field using time-resolved PIV," in *Proceedings of 15th Int. Symp. on Application of Laser Techniques to Fluid Mechanics, Lisbon, Portugal*, 2010.

[28] Tam, C. K. and Hardin, J., *Second Computational Aeroacoustics (CAA): Workshop on Benchmark Problems*, volume 3352, NASA, 1997.

[29] Gerrard, J., "An experimental investigation of the oscillating lift and drag of a circular cylinder shedding turbulent vortices," *Journal of Fluid Mechanics*, 11(02), pp. 244–256, 1961.

[30] Williams, J. F. and Hawkings, D. L., "Sound generation by turbulence and surfaces in arbitrary motion," *Philosophical Transactions of the Royal Society of London A: Mathematical, Physical and Engineering Sciences*, 264(1151), pp. 321–342, 1969.